Journal of Cleaner Production 272 (2020) 122325

Contents lists available at ScienceDirect

Journal of Cleaner Production

journal homepage: www.elsevier.com/locate/jclepro

Operating pH influences homogeneous calcium carbonate granulation in the frame of CO_2 capture

Mark Daniel G. de Luna [a, b, *], Arianne S. Sioson [b, c], Angelo Earvin Sy Choi [d], Ralf Ruffel M. Abarca [b], Yao-Hui Huang [e], Ming-Chun Lu [f, **]

[a] Department of Chemical Engineering, University of the Philippines Diliman, Quezon City, 1101, Philippines
[b] Environmental Engineering Program, National Graduate School of Engineering, University of the Philippines Diliman, Quezon City, 1101, Philippines
[c] Department of Science and Technology, Cagayan de Oro City, 9000, Philippines
[d] University Core Research Center for Disaster-free and Safety Ocean City Construction, Busan, 49315, Republic of Korea
[e] Department of Chemical Engineering, National Cheng Kung University, Tainan, 70101, Taiwan
[f] Department of Environmental Resources Management, Chia Nan University of Pharmacy and Science, Tainan, 71710, Taiwan

ARTICLE INFO

Article history:
Received 23 November 2019
Received in revised form
14 April 2020
Accepted 15 May 2020
Available online 27 June 2020

Handling editor: Xin Tong

Keywords:
Alkalinity
Carbonate recovery
Fluidized-bed reactor
Granule characteristics
Greenhouse gas mitigation

ABSTRACT

The era of industrialization has caused the drastic increase in atmospheric carbon dioxide concentrations that now require various remediation strategies such as CO_2 capture and storage. In this study, calcium carbonate granulation is proposed as a new conversion route for CO_2 trapped in water matrices into dense solids. Herein, we demonstrate the effectiveness of the fluidized-bed reactor to produce compact calcium carbonate pellets from captured CO_2 via a granulation reaction at different pH conditions and in the absence of seed materials. Constant values of calcium-to-carbonate ratio, influent carbonate concentration and influx flow rate were used while operating pH was varied from 8.5 to 11.0. Optimal operating condition with carbonate removal and granulation efficiencies of 92% and 90%, respectively was found at pH of 10.0 ± 0.2, where the lowest daily effluent concentration of carbonate ions was measured at 16.6 mg L^{-1} via the alkalinity test. At optimum operating pH, large compact granules ranging from 1 − 2 mm in diameter (~93.6 g) were obtained with overall particle size distribution leaning towards bigger sizes. Morphological analyses of the granules revealed their smooth surfaces and subrounded shapes, while crystalline and elemental analyses identified these as high purity calcium carbonate. Moreover, spontaneous homogeneous nucleation, particle aggregation, crystal growth and granulation are proposed as the main mechanisms of calcium carbonate granulation.

1. Introduction

Human activities that alter the natural carbon cycle with large CO_2 emissions and those that deplete the natural sinks of gaseous CO_2 are considered major contributors to climate change (Hu et al., 2018; Kumar et al., 2018; Matson et al., 2010). For example, global atmospheric CO_2 concentrations have steadily increased since the start of the industrial era from an annual average of 280 ppm in the late 1700s to 408 ppm by 2017, and is projected to increase by 60% in 2100 (Kumar et al., 2018; Nogalska et al., 2018). Hence, drastic reductions in industrial CO_2 emissions are needed to curb the rapid accumulation of greenhouse gases in the atmosphere. Lowering atmospheric CO_2 concentrations by other means, however, can also mitigate the long-term adverse effects of climate change.

One viable strategy to reduce CO_2 concentration in the atmosphere is by carbon capture and storage or CCS (Seipp et al., 2017). Conventional CCS technology traps, transports and stores CO_2 in depleted underground oil and gas fields or in deep saline aquifer formations. CCS processes may also employ enzymes (Sahoo et al., 2018), membranes (Nogalska et al., 2018), bacteria (Kumar et al., 2018), polymers (Shao et al., 2018), activated carbon (Boujibar et al., 2018) and amines (Kang et al., 2018). However, conventional CO_2 capture methods suffer from high temperature and energy requirements, solvent degradation, equipment corrosion, and large expensive equipment (Worathanakul and Tobarameekul,

* Corresponding author. Department of Chemical Engineering, University of the Philippines Diliman, Quezon City, 1101, Philippines.
** Corresponding author. Department of Environmental Resources Management, Chia Nan University of Pharmacy and Science, Tainan, 71710, Taiwan.
E-mail addresses: mgdeluna@up.edu.ph (M.D.G. de Luna), mmclu@mail.cnu.edu.tw (M.-C. Lu).

https://doi.org/10.1016/j.jclepro.2020.122325
0959-6526/

2016). Despite the promising results of CCS studies through the years, their application remains limited to particular storage sites with inadequate economic benefits (Sahoo et al., 2018). Thus, researches that trap and convert gaseous CO_2 into high-value products such as fuels or mineral carbonates are gaining traction in recent years (Song et al., 2018). Specifically, calcium carbonate precipitation is a promising CO_2 sequestration route because it is energy-efficient and economical (Kang et al., 2018). In addition, calcium carbonate is an essential raw material in the manufacture of cement, paper, glass and steel (Teir et al., 2005).

The purity, density and size of calcium carbonate recovered via precipitation reactions may vary depending on the specific technique used such as: (i) reactor with two chemical precursors (Wang et al., 2013), (ii) high pressure jet homogenizer for effective solution mixing (Casanova and Higuita, 2011) and (iii) gas-to-liquid diffusion (Xu et al., 2004). Some principles of the aforementioned strategies inspired the development of homogeneous calcium carbonate granulation in a fluidized-bed reactor. Fluidized-bed homogenous granulation promotes adequate mixing of reactants and solids, efficient heat and mass transfer rates, high material recovery in terms of purity, density and size, and eliminates sludge production (Chen et al., 2015; Lertratwattana et al., 2019; Salcedo et al., 2015; Udomkitthaweewat et al., 2019; Wei, 2009). Thus, understanding the factors affecting homogeneous calcium carbonate granulation is an important step to achieve efficient conversion of gaseous CO_2 into dense solids (Sioson et al., 2020).

Solution pH is a critical parameter in several CO_2 capture processes. For example, CO_2 conversion to bioplastic via fermentation relied on optimal solution pH to control the rate of bacterial growth (Al Rowaihi et al., 2018). In CO_2 amine absorption by calcium hydroxide, solution pH altered the electrical charges of amines during solvent regeneration (Kang et al., 2018). In an enzyme-based process, solution pH and temperature influenced CO_2 capture efficiency (Sahoo et al., 2018). Low pH levels promoted high bicarbonate concentrations in solution while Ca—CO_3 binding strength was found to be pH-dependent and led to the formation of different $CaCO_3$ polymorphs (Hu et al., 2015). Equilibrium and kinetic reactions of the calcium carbonate system are shown in Eqs. (1) – (7) (Gebrehiwet et al., 2014) and pH is an important parameter as it affects the generation of dominant ions such as bicarbonates, carbonates and hydroxides (Skoog and West, 1963).

$$H^+ + HCO_3^- = CO_2\,(aq)\ \log Ke_q = 6.341 \quad (1)$$

$$HCO_3^- = H^+ + CO_3^{2-}\ \log Ke_q = -10.325 \quad (2)$$

$$Ca^{2+} + HCO_3^- = H^+ + CaCO_3(aq)\ \log Ke_q = -7.009 \quad (3)$$

$$Ca^{2+} + HCO_3^- = CaHCO_3\ \log Ke_q = -0.653 \quad (4)$$

$$Ca^{2+} + H^+ = CaOH\ \log Ke_q = -12.85 \quad (5)$$

$$-\ H^+ = OH^-\ \log Ke_q = -13.991 \quad (6)$$

$$Ca^{2+} + HCO_3^- = H^+ + CaCO_3(s)\ \log Ke_q = 1.8487 \quad (7)$$

Carbon sequestration via calcium carbonate granulation involves a two-step process: (1) absorption of gaseous CO_2 into water matrices by potassium hydroxide and (2) conversion of absorbed CO_2 into calcium carbonate granules. The first step has already been extensively explored and the results showed high efficiencies for CO_2 capture (Borhani and Wang, 2019; Ramezani et al., 2017; Zarei et al., 2019). CO_2 dissolution in water by potassium hydroxide absorption was also found to be pH dependent (Sepehri et al., 2020). In the presence of potassium hydroxide, gaseous CO_2 is converted to HCO_3^- and subsequently forms K_2CO_3 (Zevenhoven et al., 2019). The second step is the focus of the present study.

Herein, the main goal is to determine the optimum pH condition that will convert trapped CO_2 in water matrices into compact calcium carbonate pellets with favorable characteristics via homogeneous granulation in a fluidized bed reactor. Separate solutions of carbonate and calcium ions were continuously introduced at opposite inlets of the reactor. The influence of operating pH on carbonate removal efficiency (C_R), carbonate granulation efficiency (C_G), carbonate fines fraction (C_{FF}) and granule characteristics were examined. Collected calcium carbonate pellets were characterized by particle size distribution, surface morphology, crystalline structure, and elemental composition.

2. Materials and methods

2.1. Chemicals and solutions

Analytical grade chemicals and reagents were used as received in all experiments. Calcium hydroxide ($Ca(OH)_2$, 90%), potassium carbonate (K_2CO_3, 99.5%), nitric acid (HNO_3, 70%) and phenolphthalein ($C_{20}H_{14}O_4$, 1%) were procured from New Star Instrument, Taiwan. Sodium hydroxide (NaOH, 98%) was purchased from the Formosa Plastic Corporation, Taiwan while sulfuric acid (H_2SO_4, ~98%) was obtained from PanReac AppliChem. Meanwhile, methyl orange ($C_{14}H_{14}N_3NaO_3S$, 0.1%) was acquired from Riedel-de Haën. All solutions were prepared using RODA ultrapure reverse osmosis water with resistance of 18.2 MΩ. The list of chemicals and reagents used in the study are summarized in Table 1.

2.2. Fluidized-bed reactor

Fig. 1 shows the schematic of the fluidized bed system used in all homogeneous $CaCO_3$ granulation runs. The cylindrical glass reactor had a working volume of 550 mL (Chen et al., 2015). Its upper section or effluent region had a height and inner diameter of 15 and 4 cm, respectively while its lower section or reaction region had a height and inner diameter of 80 and 2 cm, respectively. The increase in cross-sectional flow area from the reaction region to the effluent region reduces the upflow velocity and allows only very fine particles to go out of the reactor with the effluent. The reactor bottom had two horizontal inlets for precipitant and carbonate solutions, and one vertical inlet for effluent recirculation. The glass beads placed at the reactor bottom (i) ensured even distribution of liquid flow into the reaction region, (ii) prevented clogging and bubble formation, and (iii) provided support for the settling granules. A nomenclature of essential terms and symbols used throughout the manuscript is provided in Table 2.

2.3. Granulation experiments

Before the start of each run, ultrapure water of about 450 mL was poured into the reactor until the liquid reached the effluent port. This is done to prevent bubble formation within the reactor. The precipitant and carbonate solutions were $Ca(OH)_2$ and K_2CO_3, respectively. The experiment variables and their corresponding values are listed in Table 3 where $[Ca^{2+}]/[CO_3^{2-}]$ is the ratio between the molarities of calcium and carbonate ions, while Q_T is the sum of the influx flow rates of calcium and carbonate solutions. The following operating parameters were maintained at constant values in all runs: (i) calcium-to-carbonate molar ratio ($[Ca^{2+}]/[CO_3^{2-}] = 1.5$, (ii) total influx flow rate (Q_T) = 60 mL min^{-1} and (iii) influent carbonate concentration (C_{in}) = 10 mM. Meanwhile, the initial reflux flow rate (Q_R) was set to 30 mL min^{-1} and was then increased at a rate of 10 mL min^{-1} every 12 h until a final flow rate

Table 1
Chemicals and reagents used.

Manufacturer	Chemical name	Chemical formula	Purity
New Start Instrument	Calcium hydroxide	$Ca(OH)_2$	90%
	Potassium carbonate	K_2CO_3	99.5%
	Nitric acid	HNO_3	70%
	Phenolphthalein solution	$C_{20}H_{14}O_4$	1%
Formosa Plastic Corporation	Sodium hydroxide	NaOH	98%
PanReac AppliChem	Sulfuric acid	H_2SO_4	95%–98%
Riedel-de Haën	Methyl orange	$C_{14}H_{14}N_3NaO_3S$	0.01%

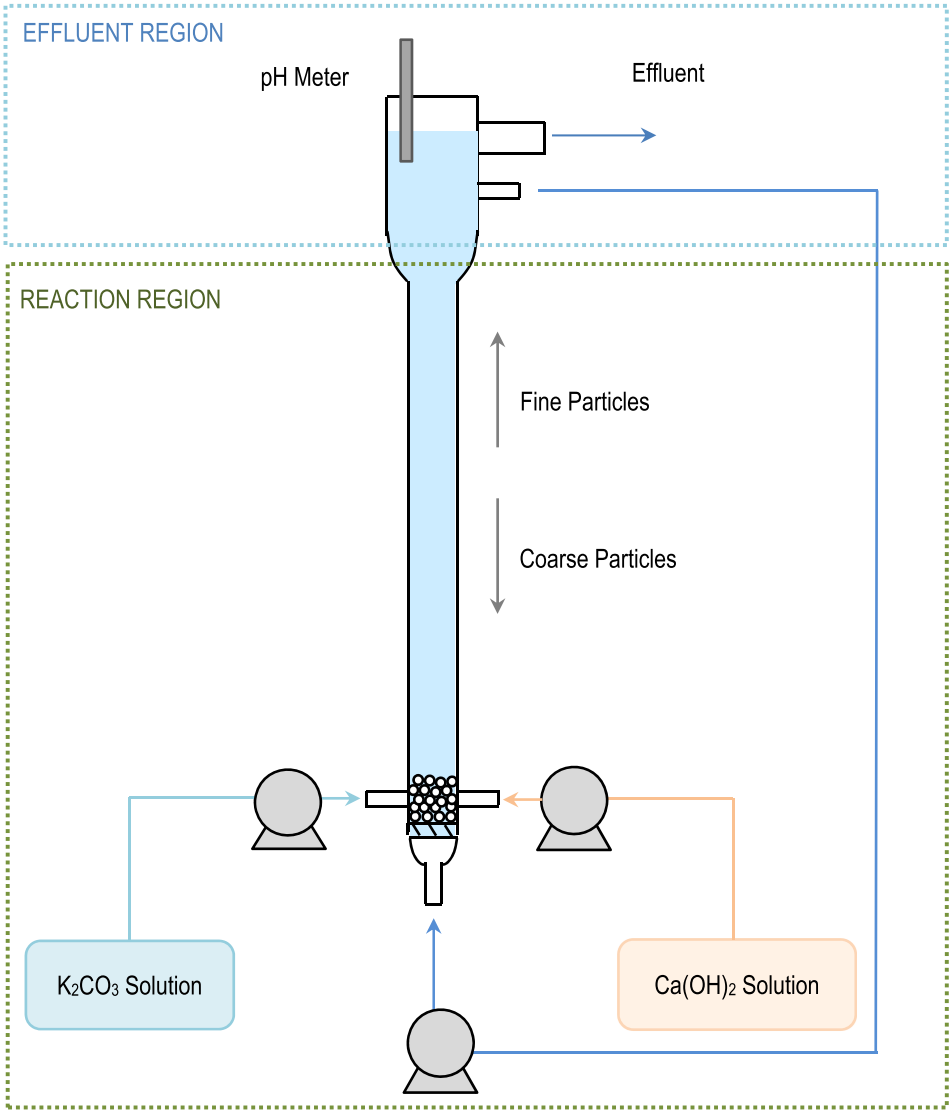

Fig. 1. Scheme of the fluidized-bed reactor for homogeneous calcium carbonate granulation.

of 100 mL min^{-1} was reached. The different operating pH (deviation of ± 0.2) evaluated in the study: 8.5, 9.0, 9.5, 10.0, 10.5 and 11.0 were controlled by the pH (deviation of ± 0.05) of the K_2CO_3 solution: 10.70, 11.00, 11.05, 11.20, 11.30 and 11.50, respectively. The pH of the $Ca(OH)_2$ solution ($S_{Ca(OH)_2}$ pH), on the other hand, was maintained at 8.00 ± 0.05. Adjustments in solution pH were done with the addition of NaOH or HNO_3 to K_2CO_3 and $Ca(OH)_2$ solutions as needed. Operating pH was monitored by a pH meter/ORP controller PC-310 (accuracy: ± 0.01 pH) procured from Shin Shiang Tech Instruments.

Each granulation run lasted for 168 h. During the first 20 h, samples were drawn from the effluent every 2 h and thereafter every 24 h. At predetermined intervals, two 100 mL samples were drawn: one was unfiltered while the other was filtered using a 0.45 μm microsyringe filter. All samples were analyzed for C_R, C_G, C_{FF} and C_{WF} following Eqs. (8) – (11), respectively. Of these parameters, C_R determines the concentration of carbonate removed and precipitated, C_G quantifies the conversion of carbonate into either sludge or granules, and C_{FF} defines the dominant mechanism of granulation whether favoring nuclei production or granule

Table 2
Symbols, terms and units.

Symbol	Meaning	Unit
Q_{CO_3}	Carbonate influx flow rate	mL min^{-1}
Q_{Ca}	Calcium influx flow rate	mL min^{-1}
Q_T	Total influx flow rate	mL min^{-1}
Q_R	Reflux flow rate	mL min^{-1}
C_{in}	Influent carbonate concentration	mM
C_d	Dissolved effluent carbonate concentration	mM
C_t	Total effluent carbonate concentration	mM
C_f	Effluent carbonate fines concentration	mM
C_R	Carbonate removal efficiency	%
C_G	Carbonate granulation efficiency	%
C_{FF}	Carbonate fines fraction	%
C_{WF}	Carbonate granules weight fraction	%
W_{ms}	Weight of granules collected in every mesh size	g
W_t	Total weight of granules collected	g
Operating pH	Effluent pH	
$[Ca^{2+}]/[CO_3^{2-}]$	Calcium-to-carbonate ratio	

formation. In all experiments, efficiencies were calculated from the average alkalinity measurements taken throughout each run.

$$\%C_R = \left(1 - \frac{C_d \cdot Q_T}{C_{in} \cdot Q_{CO_3}}\right) \cdot 100 \quad (8)$$

$$\%C_G = \left(1 - \frac{C_t \cdot Q_T}{C_{in} \cdot Q_{CO_3}}\right) \cdot 100 \quad (9)$$

$$\%C_{FF} = \frac{C_f}{C_{in}} \cdot 100 \quad (10)$$

$$\%C_{WF} = \frac{W_{ms}}{W_t} \cdot 100 \quad (11)$$

2.4. Analytical methods

Total and dissolved carbonate concentrations were determined by "Total Alkalinity Buret Titration" and "Hach Method 8221 − Phenolphthalein" (instrumental accuracy of 0.2%), respectively. These titrimetric methods of analysis are prescribed by the United States Environmental Protection Agency − National Pollutant Discharge Elimination System. Specifically, N/50 H_2SO_4 was used as titrant while phenolphthalein and methyl orange were employed as indicators for phenolphthalein and total alkalinity, respectively. Carbonate, bicarbonate and hydroxide concentrations were determined from phenolphthalein and total alkalinity measurements.

Large granules obtained from each run were properly characterized. The surface morphologies of the granules were evaluated using an FEI Quanta 200 Environmental Scanning Electron Microscope (SEM) with a resolution of 3 nm. The crystalline properties of the granules were analyzed by X-ray diffraction (XRD) using a Multi-function X-ray Diffractometer with an angular resolution of 0.012°. The elemental composition of the granules was determined by energy dispersive X-ray (EDX) spectroscopy. The granule size distribution for each run was analyzed using Tyler sieves of varying mesh diameters: 0.149, 0.297, 0.42, 0.5, 0.59, 1 and 2 mm. The weight of each size fraction and the cumulative weight were utilized to generate the particle size distribution of the granules.

3. Results and discussion

3.1. Effect of operating pH on effluent alkalinity

Alkalinity is the capacity of bicarbonate, carbonate and hydroxide ions in water matrices to neutralize acids, with solution pH dictating the major form of alkalinity in the system (Chen et al., 2000). The alkalinity of water is usually determined by phenolphthalein and total alkalinity tests, and the results are reported in mg L^{-1} $CaCO_3$. Equilibrium equations of the alkalinity of carbonate solutions are shown in Eqs. (12)–(15) (Lower, 1996) where ion concentrations enclosed in brackets are molar concentrations.

$$\frac{[H^+][HCO_3^-]}{[H_2CO_3^*]} = K_1 = 10^{-6.3},\ pK_1 = 6.3 \quad (12)$$

$$\frac{[H^+]\left[CO_3^{2-}\right]}{[HCO_3^-]} = K_2 = 10^{-10.3},\ pK_2 = 10.3 \quad (13)$$

$$[H^+][OH^-] = K_w = 10^{-14} \quad (14)$$

$$[\text{Total alkalinity}] = [HCO_3^-] + 2\left[CO_3^{2-}\right] + [OH^-] - [H^+] \quad (15)$$

Carbonic acid concentration, $[H_2CO_3^*]$ accounts for the total concentration of dissolved CO_2 and H_2CO_3. The forms of alkalinity in the system depend on (i) the pH of the solution and (ii) the pKa of the carbonate species or the pH at which the chemical species will accept or donate a proton. When the value of pKa is greater than pH, the extent of dissociation of the chemical species in solution is reduced.

Residual concentrations of HCO_3^-, CO_3^{2-} and OH^- ions in the effluent at different operating pH are shown in Fig. 2. At operating pH = 8.5, HCO_3^- ions was the dominant form of alkalinity in the effluent and CO_3^{2-} only appeared during the first 12 h of the run. Operating pH exceeded the set pH value at the beginning of the run due to the unstable reactions in the reactor. When the reactant and the precipitant were mixed, there was a sudden appearance of a smoke-like fluid which travelled upwards from the point of contact between the reactants. The smoke-like fluid was the visible manifestation of spontaneous nucleation resulting from the chemical reaction between carbonate and calcium ions. The generated calcium carbonate nuclei eventually passed from semisolid to solid state, agglomerated with other nuclei and formed into granules (Chen et al., 2015). As the reaction proceeded from nucleation, to particle aggregation and growth, and finally to granulation, a

Table 3
Experiment variables and values.

Independent variable	Number of variation	Range of values
Calcium-to-carbonate molar ratio ($[Ca^{2+}]/[CO_3^{2-}]$)	1	1.5
Total influx flow rate (Q_T: mL min^{-1})	1	60
Influent carbonate concentration (C_{in}: mM)	1	10
Operating pH	6	8.5 − 11.0
K_2CO_3 solution pH	6	10.7 − 11.5
$Ca(OH)_2$ solution ($S_{Ca(OH)_2}$) pH	1	8

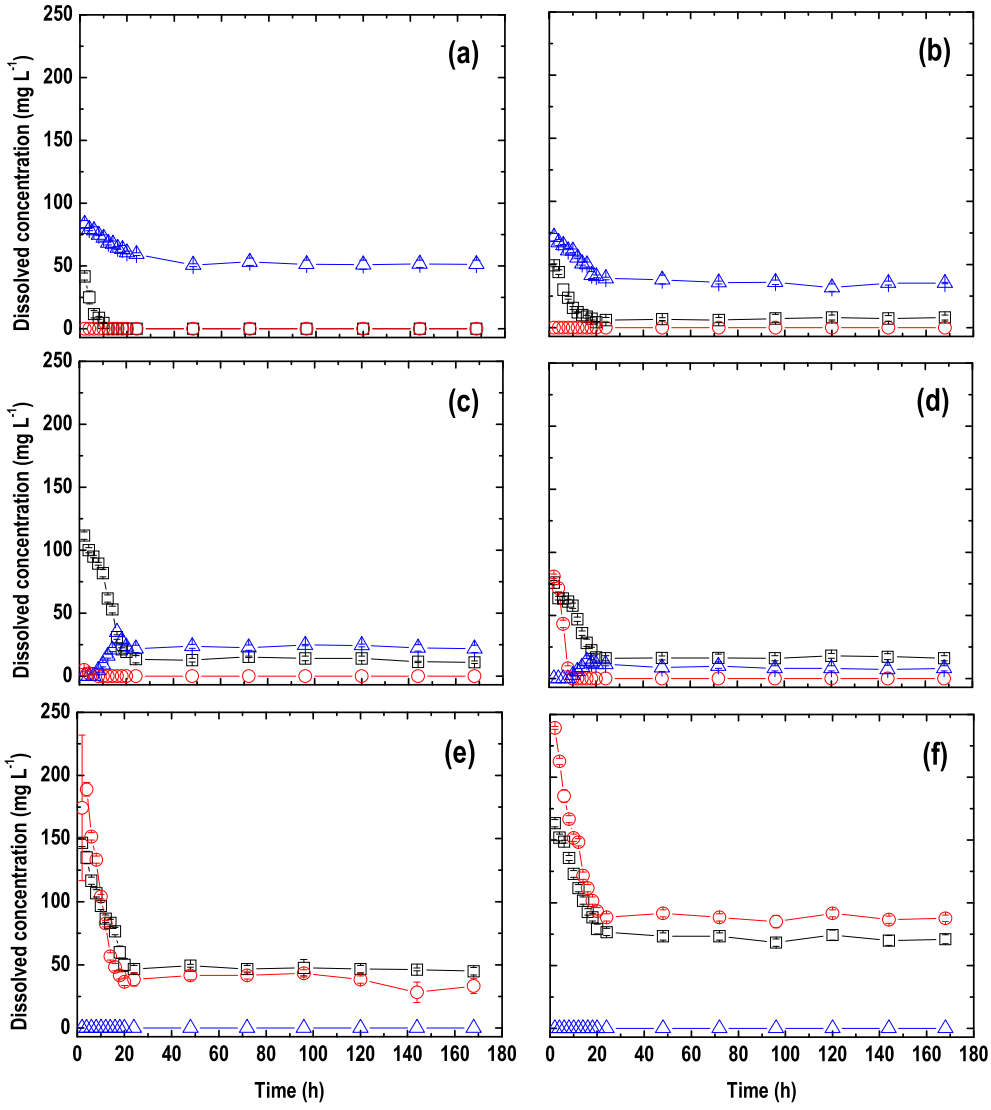

Fig. 2. Effluent concentrations of HCO_3^- —△—, CO_3^{2-} —□— and OH^- ions —○— at varying operating pH: (a) 8.5, (b) 9.0, (c) 9.5, (d) 10.0, (e) 10.5 and (f) 11.0.

decline in operating pH was noted. The operating pH became stable only when sufficient granules filled the reaction zone and some granules almost reached the effluent region. At operating pH = 9.0, traces of CO_3^{2-} ions were present throughout the run. However, HCO_3^- ions still dominated effluent alkalinity. At operating pH = 9.5, concentrations of HCO_3^- ions were higher than CO_3^{2-} ions. Nevertheless, during the first 14 h, CO_3^{2-} ions dominated the system because the operating pH favored carbonate alkalinity. At operating pH = 10.0, OH^- ions were detected during the first 8 h. Afterwards, HCO_3^- ions were produced, but at this operating pH the concentration of CO_3^{2-} ions became higher than HCO_3^- ions. At operating pH = 10.5, CO_3^{2-} and OH^- ions were the forms of alkalinity in the effluent with concentration of CO_3^{2-} ions higher than the other components. However, the concentration of OH^- ions during the first 8 h exceeded those of CO_3^{2-} ions. This increase in hydroxide concentrations is attributed to the combined effects of the precipitant, $Ca(OH)_2$ and the NaOH used for pH adjustments. Lastly, at operating pH = 11.0, the concentration of OH^- ions were higher than CO_3^{2-} ions throughout the run and this is due to the very large volume of NaOH solution required to achieve the desired operating pH. Therefore, OH^- ions from NaOH and $Ca(OH)_2$ solutions had a high impact on hydroxide alkalinity in the effluent. Overall, operating pH between pK_1 and pK_2 indicated the dominance of HCO_3^- ions, while CO_3^{2-} ions prevailed at operating pH greater than pK_2 and a further increase in operating pH led to the proliferation of OH^- ions in the system (Skoog and West, 1963).

The HCO_3^- and OH^- ions did not co-exist in the water matrix due to their instantaneous reaction to form CO_3^{2-} ions (Panchagnula and Charan singh, 2016). Therefore, it can be inferred that the individual ions of HCO_3^-, CO_3^{2-} and OH^- are unable to co-exist in solution (Panchagnula and Charan singh, 2016). The calculation of the primary forms of alkalinity in the effluent was needed to determine the concentrations of HCO_3^- and CO_3^{2-} ions. These were used as the basis for the computation of carbonate removal and granulation efficiencies.

3.2. Effect of operating pH on carbonate removal and granulation

For each run, the removal and granulation efficiencies improved with time and stabilized when the granules reached the upper

portion of the reaction region (Caddarao et al., 2018). However, granules reaching the reflux flow outlet need to be removed to prevent unnecessary clogging of the outlet.

Fig. 3 shows that operating pH influenced carbonate removal and granulation efficiencies. While homogeneous $CaCO_3$ granulation occurs at basic pH, granulation and dissolution of $CaCO_3$ also depends on carbonate supersaturation (Ayoub et al., 2014). Granulation of $CaCO_3$ was easier and faster at higher supersaturation (Zarga et al., 2014). Lower supersaturation allows the chemical species to move freely in solution with minimal or no collisions with other species and this results in inhibited nuclei agglomeration and increased porosity in the resulting granules (Aldaco et al., 2007). As operating pH is increased, the efficiencies of carbonate removal and granulation are also increased. At higher supersaturation, more ions of calcium and carbonate interacted and formed into discrete nuclei and these particles agglomerated and subsequently grew into granules. The presence of higher amounts of $CaCO_3$ triggered stronger interactions among particles to form more compact and smoother granules (Sioson et al., 2020). This was driven by greater supersaturation as a result of high pH levels. Highest efficiencies with the smallest delta were obtained at operating pH = 10.0 with C_R = 92% and C_G = 90%. However, further increasing the operating pH decreased the removal and granulation efficiencies and increased the delta of the two efficiencies (Mahasti et al., 2017). The delta determines the amount of granulated calcium carbonate that remained within the reactor. The larger the delta, the greater the concentration of fines released at the effluent. High operating pH (> 11.0) can lead to the production of sludge due to the favorable precipitation of gelatinous calcium hydroxide (Oncel et al., 2013). C_{FF} had an inverse relationship with carbonate removal and granulation efficiencies. When the efficiencies increased, the fines fraction decreased. When the C_{FF} was low, the effluent was clear and had minimal $CaCO_3$ particles discharged in the effluent. Low C_{FF} of 1% is desired, which was obtained at operating pH = 10.0.

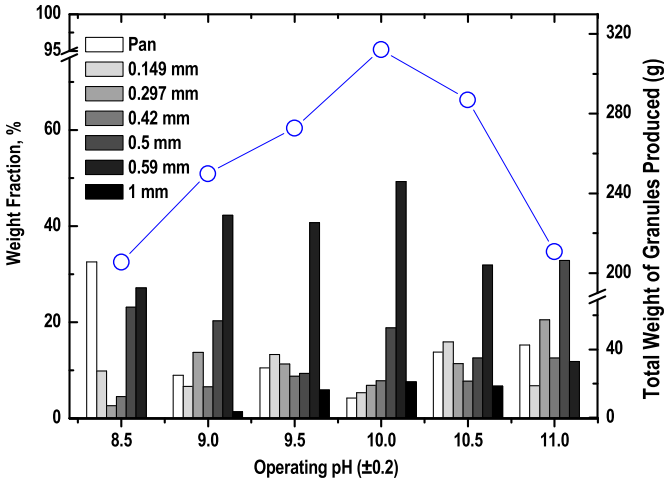

Fig. 4. Effect of operating pH on W_T —○— and particle size distribution of collected granules.

Operating pH significantly influenced the degree of granulation and dissociation of $CaCO_3$ in solution. Granulation at operating pH < 10.0 favored the formation of bicarbonate ions and therefore decreased $CaCO_3$ granulation. At operating pH > 10.0, however, the concentration of hydroxide ions in the water matrix is increased. The hydroxide ions reacted with calcium ions to form $Ca(OH)_2$ particles that compromised the structural integrity of the calcium

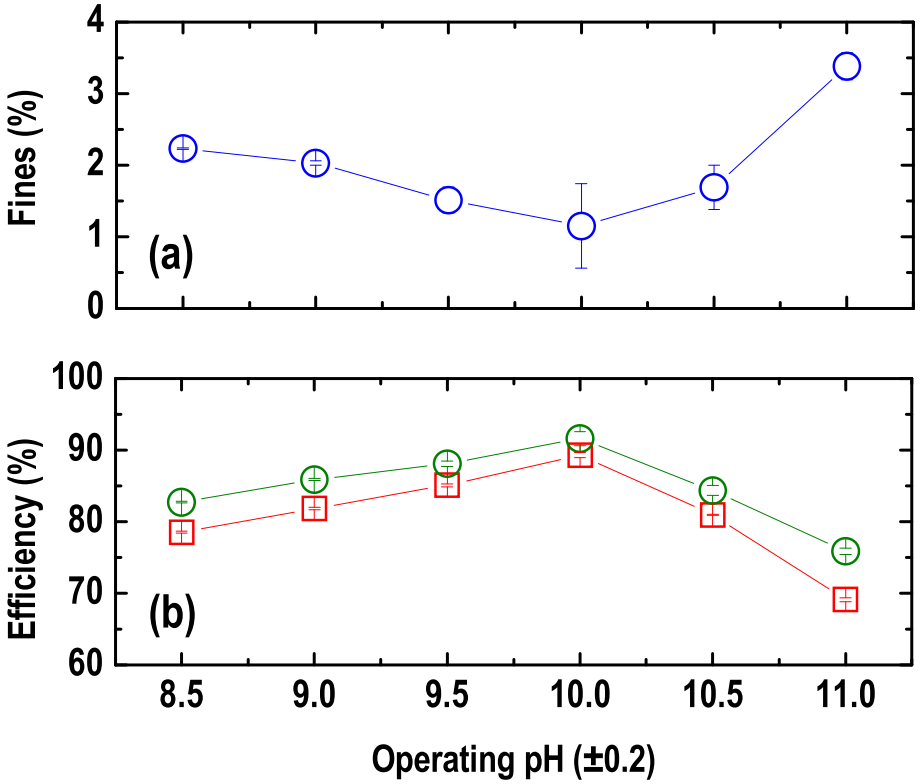

Fig. 3. Effect of operating pH on (a) $[Carbonate]_{FF}$ —○—, and (b) $[Carbonate]_R$ —○— and $[Carbonate]_G$—□—.

carbonate granules. Overall, the concentration of carbonate ions dictated the efficiency of $CaCO_3$ granulation (Declet et al., 2016).

3.3. Effect of operating pH on granule size distribution

Fig. 4 shows the cumulative weights of the collected granules at the end of each run and the corresponding size distributions of the granules as functions of operating pH. Large granules with diameters between 1.0 – 2.0 mm weighing ~93.6 g were obtained at optimal operating pH = 10.0. The large granules account for approximately 8% of the total weight of the granules collected at optimal operating pH. In addition, the size distribution of these granules leaned towards larger sizes and can be described by the normal-inverse Gaussian and the generalized hyperbolic distribution curves (Caddarao et al., 2018; Sorensen et al., 2016). Thus, a decrease or increase in operating pH from pH 10.0 resulted in the decline in the size of granules and the proliferation of smaller granules with diameters below 0.5 mm.

At operating pH = 8.5, about 73% of the granules collected had diameters less than 0.59 mm. At this condition, the formation of HCO_3^- ions is favored, which hindered $CaCO_3$ nucleation and granulation. Hence, none of the granules recovered reached 1 mm in diameter. However, granules collected at operating pH = 9.0, 9.5, 10.0 and 10.5, contained large granules with diameters between 1.0 and 2.0 mm. In all the runs, the amount of granules recovered with diameters greater than 1.0 mm was highest at 8% and those below 0.59 mm was lowest at 43%; these granules were obtained at operating pH = 10.0. At operating pH = 9.0, 9.5 and 10.5, nucleation prevailed over granuation. This is validated by the size distribution of the granules which leaned towards more and faster production

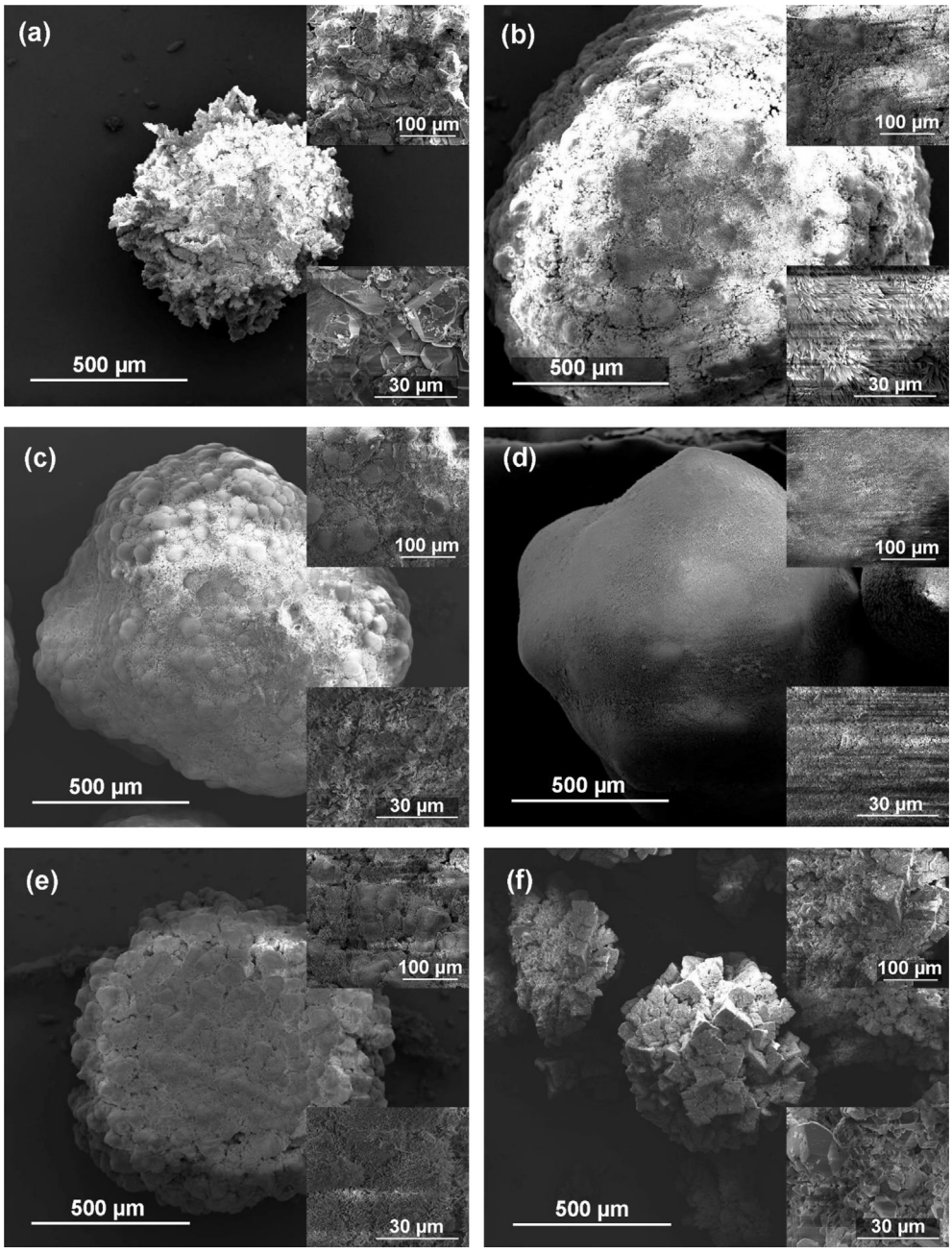

Fig. 5. SEM images of granules at varying operating pH: (a) 8.5, (b) 9.0, (c) 9.5, (d) 10.0, (e) 10.5 and (f) 11.0.

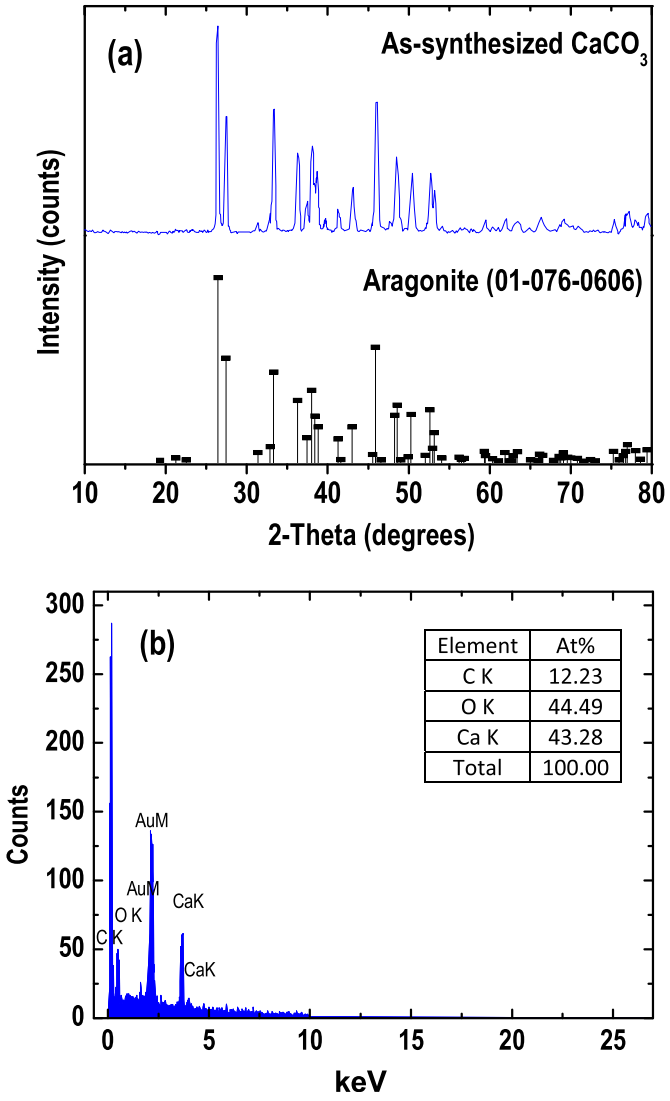

Fig. 6. Graphs showing (a) XRD pattern and (b) EDX spectrum of granules obtained at operating pH = 10.

of granules with diameters below 0.59 mm. At operating pH = 11.0, no granules with diameters between 1.0 − 2.0 mm were recovered and 88% of the granules collected had diameters below 0.59 mm. This is attributed to the high concentration of OH^- ions that co-precipitated $Ca(OH)_2$.

The results also showed the direct proportional relationship between the cumulative weights of the granules and their corresponding particle size distributions from pH 8.5 to 10.0. At this pH range, the experiments with larger collected granules, having diameters between 1.0 − 2.0 mm had higher yields in total weight. The granules with the highest yield of 312.2 g were obtained at operating pH =10.0. The production of granules with sizes from 1.0 to 2.0 mm was a good indication of $CaCO_3$ nucleation and growth that resulted in higher removal and granulation efficiencies. The large granules obtained in each of the runs were analyzed for their physical and chemical properties.

3.4. Effect of operating pH on granule characteristics

Fig. 5 shows the electronic images of recovered $CaCO_3$ granules under different magnifications. The mechanisms of granule formation can be inferred from the SEM micrographs as follows: nucleation, aggregation, crystal growth and granulation. Nevertheless, the surface morphologies of the granules varied at different operating pH. All the granules, however, appeared to have sub-rounded shapes. Some granules had small cracks and crevices and were hollow within while others were compact and dense. Most were rough on the surface and a few were noticeably smooth. At operating pH = 8.5 (Fig. 5a), the large granules collected had diameters below 0.59 mm. Nucleation was the dominant mechanism at this pH condition which favored the production of small granules, and the effective growth area of the granules remained unchanged (Tadros et al., 1976). Homogeneous granulation at operating pH = 9.0 resulted in hollow granules. As shown in Fig. 5b, small pores are clearly distributed on the granule surface. The spiky outer surface of the granule is more evident at 10,000× magnification. The granules collected at operating pH = 9.5 (Fig. 5c) and 10.0 (Fig. 5d) had no visible openings. However, the granules recovered at operating pH = 10.0 had smoother surfaces than those obtained at pH = 9.0. At operating pH = 10.5 (Fig. 5e), pores and other openings permeated the outer surface of the granules. Hydroxide alkalinity was measured in the effluent at this pH condition. At operating pH = 11.0 (Fig. 5f), small and fragile granules were collected. Although bigger granules were noted inside the reactor at this pH condition, the granules eventually crumbled into smaller fragments when these were collected and dried leaving behind irregularly-shaped solids with uneven surfaces. This can be explained by the co-precipitation of $Ca(OH)_2$, a compound with no mechanical strength, which affected the structural integrity of the resulting granules (Nicholson and Czarnecka, 2016).

Dense, compact and smooth-surfaced granules were only obtained at optimum operating conditions where: operating pH = 10, $[Ca^{2+}]/[CO_3^{2-}] = 1.5$, $C_{in} = 10$ mM, and $Q_T = 60$ mL min^{-1}. When operating pH was set below the optimum value, $CaCO_3$ granulation was inhibited because the polycompound became more protonated and less charged. Moreover, increasing the operating pH beyond 10.0 hindered $CaCO_3$ precipitation due to the decreased surface charge density and the destruction of chemical bonds (Declet et al., 2016). At optimal operating pH, the reaction between the carbonate centers with calcium ions produced small nuclei within the reaction zone during the first few minutes of each run. These particles then aggregated into a critical nuclei which increased in size and eventually formed into $CaCO_3$ granules (Chen et al., 2015; Salcedo et al., 2016).

Fig. 6a shows the close similarity between the diffractograms of the collected granules and pure aragonite in several major peaks, specifically at 2-theta of 26.5°, 27.5°, 33.3°, 36.4°, 38.1°, 43.1°, 46.1°, 48.5°, 50.5° and 52.7°. Moreover, the granulation runs performed at 25 °C favored aragonite formation, and the prolonged duration of each run to 168 h resulted in higher intensities of these diffraction peaks compared to pure aragonite (Ramakrishna et al., 2016). Meanwhile, the EDX spectrum of the recovered granules shown in Fig. 6b reveal only three elements: calcium (Ca), carbon (C) and oxygen (O), also the only elements comprising aragonite. No trace of other elements were detected. In addition, the ratios of the elements comprising the granules conformed to the corresponding ratios of the molecular weights of the elements in $CaCO_3$ (100.1 g mol^{-1}) with Ca = 40.1 g mol^{-1}, C = 12.0 g mol^{-1} and O = 48.0 g mol^{-1}. These results demonstrate the effectiveness of the granulation process in recovering high purity calcium carbonate granules.

4. Conclusions

The study demonstrates the effectiveness of homogeneous granulation process in producing large, compact and high-purity calcium carbonate granules from captured CO_2 using a fluidized

bed reactor. More importantly, we showed the critical role of operating pH in (i) determining the alkalinity of the water matrix, (ii) ensuring high carbonate removal and granulation efficiencies, and (iii) producing favorable granule properties such as particle size distribution, morphology, crystallinity and composition. Future research can investigate the techno-economic analysis of the homogeneous granulation process in the frame of CO_2 capture.

CRediT authorship contribution statement

Mark Daniel G. de Luna: Conceptualization, Supervision, Formal analysis, Writing - review & editing. **Arianne S. Sioson:** Conceptualization, Writing - original draft, Writing - review & editing, Visualization, Formal analysis. **Angelo Earvin Sy Choi:** Writing - original draft, Writing - review & editing, Visualization, Formal analysis. **Ralf Ruffel M. Abarca:** Visualization, Writing - review & editing. **Yao-Hui Huang:** Conceptualization, Supervision. **Ming-Chun Lu:** Conceptualization, Supervision, Funding acquisition, Formal analysis, Resources.

Declaration of competing interest

The authors declare that they have no known competing financial interests or personal relationships that could have appeared to influence the work reported in this paper.

Acknowledgement

The authors would like to thank the Ministry of Science and Technology, Taiwan (Contract No. MOST-102-2221-E-041-001-MY3) and the National Research Foundation of Korea through the Ministry of Education (No. 2016R1A6A1A03012812) for providing financial support for this research undertaking.

References

Al Rowaihi, I.S., Kick, B., Grötzinger, S.W., Burger, C., Karan, R., Weuster-Botz, D., Eppinger, J., Arold, S.T., 2018. A two-stage biological gas to liquid transfer process to convert carbon dioxide into bioplastic. Bioresour. Technol. Reports 1, 61–68. https://doi.org/10.1016/j.biteb.2018.02.007.

Aldaco, R., Garea, A., Irabien, A., 2007. Calcium fluoride recovery from fluoride wastewater in a fluidized bed reactor. Water Res. 41, 810–818. https://doi.org/10.1016/j.watres.2006.11.040.

Ayoub, G.M., Zayyat, R.M., Al-Hindi, M., 2014. Precipitation softening: a pretreatment process for seawater desalination. Environ. Sci. Pollut. Res. 21, 2876–2887. https://doi.org/10.1007/s11356-013-2237-1.

Borhani, T.N., Wang, M., 2019. Role of solvents in CO2 capture processes: the review of selection and design methods. Renew. Sustain. Energy Rev. 114, 109299. https://doi.org/10.1016/j.rser.2019.109299.

Boujibar, O., Souikny, A., Ghamouss, F., Achak, O., Dahbi, M., Chafik, T., 2018. CO2 capture using N-containing nanoporous activated carbon obtained from argan fruit shells. J. Environ. Chem. Eng. 6, 1995–2005. https://doi.org/10.1016/j.jece.2018.03.005.

Caddarao, P.S., Garcia-Segura, S., Ballesteros, F.C., Huang, Y.H., Lu, M.C., 2018. Phosphorous recovery by means of fluidized bed homogeneous crystallization of calcium phosphate. Influence of operational variables and electrolytes on brushite homogeneous crystallization. J. Taiwan Inst. Chem. Eng. 83, 124–132. https://doi.org/10.1016/j.jtice.2017.12.009.

Casanova, H., Higuita, L.P., 2011. Synthesis of calcium carbonate nanoparticles by reactive precipitation using a high pressure jet homogenizer. Chem. Eng. J. 175, 569–578. https://doi.org/10.1016/j.cej.2011.09.051.

Chen, C.S., Shih, Y.J., Huang, Y.H., 2015. Remediation of lead (Pb(II)) wastewater through recovery of lead carbonate in a fluidized-bed homogeneous crystallization (FBHC) system. Chem. Eng. J. 279, 120–128. https://doi.org/10.1016/j.cej.2015.05.013.

Chen, Y.-H., Yeh, H.-H., Tsai, M.-C., Lai, W.-L., 2000. The application of fluidized bed crystallization in drinking water softening. J. Chin. Inst. Environ. Eng. 10, 177–184.

Declet, A., Reyes, E., Suarez, O.M., 2016. Calcium carbonate precipitation: a review of the carbonate crystallization process and applications in bioinspired composites. Rev. Adv. Mater. Sci. 44, 87–107.

Gebrehiwet, T., Guo, L., Fox, D., Huang, H., Fujita, Y., Smith, R., Henriksen, J., Redden, G., 2014. Precipitation of calcium carbonate and calcium phosphate under diffusion controlled mixing. Appl. Geochem. 46, 43–56. https://doi.org/10.1016/j.apgeochem.2014.04.005.

Hu, Y. Bin, Wolthers, M., Wolf-Gladrow, D.A., Nehrke, G., 2015. Effect of pH and phosphate on calcium carbonate polymorphs precipitated at near-freezing temperature. Cryst. Growth Des. 15, 1596–1601. https://doi.org/10.1021/cg500829p.

Hu, G., Xiao, Z., Smith, K., Kentish, S., Stevens, G., Connal, L.A., 2018. A carbonic anhydrase inspired temperature responsive polymer based catalyst for accelerating carbon capture. Chem. Eng. J. 332, 556–562. https://doi.org/10.1016/j.cej.2017.09.039.

Kang, J.M., Murnandari, A., Youn, M.H., Lee, W., Park, K.T., Kim, Y.E., Kim, H.J., Kang, S.P., Lee, J.H., Jeong, S.K., 2018. Energy-efficient chemical regeneration of AMP using calcium hydroxide for operating carbon dioxide capture process. Chem. Eng. J. 335, 338–344. https://doi.org/10.1016/j.cej.2017.10.136.

Kumar, M., Sundaram, S., Gnansounou, E., Larroche, C., Thakur, I.S., 2018. Carbon dioxide capture, storage and production of biofuel and biomaterials by bacteria: a review. Bioresour. Technol. 247, 1059–1068. https://doi.org/10.1016/j.biortech.2017.09.050.

Lertratwattana, K., Kemacheevakul, P., Garcia-Segura, S., Lu, M.C., 2019. Recovery of copper salts by fluidized-bed homogeneous granulation process: high selectivity on malachite crystallization. Hydrometallurgy 186, 66–72. https://doi.org/10.1016/j.hydromet.2019.03.015.

Lower, S.K., 1996. Carbonate equilibria in natural waters. Environ. Chem.

Mahasti, N.N.N., Shih, Y.J., Vu, X.T., Huang, Y.H., 2017. Removal of calcium hardness from solution by fluidized-bed homogeneous crystallization (FBHC) process. J. Taiwan Inst. Chem. Eng. 78, 378–385. https://doi.org/10.1016/j.jtice.2017.06.040.

Matson, P.A., Dietz, T., Abdalati, W., Busalacchi, A.J.J., Caldeira, K., Corell, R.W., Defries, R.S., Fung, I.Y., Gaines, S., Hornberger, G.M., Lemos, M.C., Moser, S.C., Moss, R.H., Parson, E.A., Ravishankara, A.R., Schmitt, R.W., Turner, B.L.I., Washington, W.M., Weyant, J.P., Whelan, D.A., Kraucunas, I., 2010. National Research Council-Advancing the Science of Climate Change. The National Academies Press, Washington, DC. https://doi.org/10.17226/12782.

Nicholson, J., Czarnecka, B., 2016. Materials for the Direct Restoration of Teeth, Woodhead Publishing Series in Biomaterials. Woodhead Publishing. https://doi.org/10.1016/B978-0-08-100491-3.00009-X.

Nogalska, A., Zukowska, A., Garcia-Valls, R., 2018. Atmospheric CO2 capture for the artificial photosynthetic system. Sci. Total Environ. 621, 186–192. https://doi.org/10.1016/j.scitotenv.2017.11.248.

Oncel, M.S., Muhcu, A., Demirbas, E., Kobya, M., 2013. A comparative study of chemical precipitation and electrocoagulation for treatment of coal acid drainage wastewater. J. Environ. Chem. Eng. 1, 989–995. https://doi.org/10.1016/j.jece.2013.08.008.

Panchagnula, S., Charan singh, T., 2016. A study of alkalinity in water samples-titrimetry. Int. J. Trend Res. Dev. 3, 370–372.

Ramakrishna, C., Thenepalli, T., Huh, J.H., Ahn, J.W., 2016. Preparation of needle like aragonite precipitated calcium carbonate (PCC) from dolomite by carbonation method. J. Korean Ceram. Soc. 53, 7–12. https://doi.org/10.4191/kcers.2016.53.1.7.

Ramezani, R., Mazinani, S., Di Felice, R., Darvishmanesh, S., Van der Bruggen, B., 2017. Selection of blended absorbents for CO2 capture from flue gas: CO2 solubility, corrosion and absorption rate. Int. J. Greenh. Gas Control 62, 61–68. https://doi.org/10.1016/j.ijggc.2017.04.012.

Sahoo, P.C., Kumar, M., Puri, S.K., Ramakumar, S.S.V., 2018. Enzyme inspired complexes for industrial CO2 capture: opportunities and challenges. J. CO2 Util. 24, 419–429. https://doi.org/10.1016/j.jcou.2018.02.003.

Salcedo, A.F.M., Ballesteros, F.C., Vilando, A.C., Lu, M.C., 2016. Nickel recovery from synthetic Watts bath electroplating wastewater by homogeneous fluidized bed granulation process. Separ. Purif. Technol. 169, 128–136. https://doi.org/10.1016/j.seppur.2016.06.010.

Salcedo, A.F.M., Ballesteros, F.C.J., Lu, M.-C., 2015. Recovery of nickel from industrial wastewater by homogeneous fluidized-bed granulation: effects of influent nickel concentration, CO3: Ni ratio and pH of the precipitant. In: Proceedings of the 14th International Conference on Environmental Science and Technology, pp. 1–5.

Seipp, C.A., Williams, N.J., Kidder, M.K., Custelcean, R., 2017. CO2 capture from ambient air by crystallization with a guanidine sorbent. Angew. Chem. Int. Ed. 55, 1–5. https://doi.org/10.1002/anie.201610916.

Sepehri, A., Sarrafzadeh, M.H., Avateffazeli, M., 2020. Interaction between Chlorella vulgaris and nitrifying-enriched activated sludge in the treatment of wastewater with low C/N ratio. J. Clean. Prod. 247, 119164. https://doi.org/10.1016/j.jclepro.2019.119164.

Shao, L., Liu, M., Huang, J., Liu, Y., 2018. CO 2 capture by nitrogen-doped porous carbons derived from nitrogen- containing hyper-cross-linked polymers. J. Colloid Interface Sci. 513, 304–313.

Sioson, A.S., Choi, A.E.S., de Luna, M.D.G., Huang, Y.-H., Lu, M.-C., 2020. Calcium carbonate granulation in a fluidized-bed reactor: kinetic, parametric and granule characterization analyses. Chem. Eng. J. 382, 122879. https://doi.org/10.1016/j.cej.2019.122879.

Skoog, D.A., West, D.M., 1963. Fundamentals of analytical chemistry. J. Chem. Educ. 40, 614. https://doi.org/10.1021/ed040p614.2.

Song, X., Wu, Y., Pan, D., Wei, R., Gao, L., Zhang, J., Xiao, G., 2018. Melem based multifunctional catalyst for chemical fixation of carbon dioxide into cyclic carbonate. J. CO2 Util. 24, 287–297. https://doi.org/10.1016/j.jcou.2018.01.017.

Sorensen, M., Podolskij, Stelzer, Thorbjørnsen, Veraart, 2016. On the Size Distribution of Sand, the Fascination of Probability, Statistics and Their Applications.

Springer, Cham. https://doi.org/10.1007/978-3-319-25826-3_1.
Tadros, M.E., Skalny, J.A.N., Kalyoncu, R.S., 1976. Kinetics of calcium hydroxide crystal growth from solution. J. Colloid Interface Sci. 55, 20–24.
Teir, S., Eloneva, S., Zevenhoven, R., 2005. Production of precipitated calcium carbonate from calcium silicates and carbon dioxide. Energy Convers. Manag. 46, 2954–2979. https://doi.org/10.1016/j.enconman.2005.02.009.
Udomkitthaweewat, N., Anotai, J., Choi, A.E.S., Lu, M.C., 2019. Removal of zinc based on a screw manufacturing plant wastewater by fluidized-bed homogeneous granulation process. J. Clean. Prod. 230, 1276–1286. https://doi.org/10.1016/j.jclepro.2019.05.192.
Wang, H., Huang, W., Han, Y., 2013. Diffusion-reaction compromise the polymorphs of precipitated calcium carbonate. Particuology 11, 301–308. https://doi.org/10.1016/j.partic.2012.10.003.
Wei, Z., 2009. A review of techniques for the process intensification of fluidized bed reactors. Chin. J. Chem. Eng. 17, 688–702. https://doi.org/10.1016/S1004-9541(08)60264-5.
Worathanakul, P., Tobarameekul, P., 2016. Development of NaY zeolite derived from biomass and environmental assessment of carbon dioxide reduction. In: International Conference on Chemical and Food Engineering, pp. 1–5. https://doi.org/10.1051/matecconf/20166206003.
Xu, X., Han, J.T., Cho, K., 2004. Formation of amorphous calcium carbonate thin films and their role in biomineralization. Chem. Mater. 16, 1740–1746. https://doi.org/10.1021/cm035183d.
Zarei, A., Hafizi, A., Rahimpour, M.R., Raeissi, S., 2019. Carbon dioxide absorption into aqueous potassium salt solutions of glutamine amino acid. J. Mol. Liq. 111743 https://doi.org/10.1016/j.molliq.2019.111743.
Zarga, Y., Elfil, H., Ben Boubaker, H., 2014. Calcium sulfate and calcium carbonate simple and mixed precipitations. J. New Sci. 8, 7–16.
Zevenhoven, R., Legendre, D., Said, A., Järvinen, M., 2019. Carbon dioxide dissolution and ammonia losses in bubble columns for precipitated calcium carbonate (PCC) production. Energy 175, 1121–1129. https://doi.org/10.1016/j.energy.2019.03.112.